The structure of C_2H_4 clusters from theoretical interaction potentials and vibrational predissociation data

R. Ahlrichs[1], S. Brode[1,*], U. Buck[2], M. DeKieviet[2,], Ch. Lauenstein[2,***], A. Rudolph[2], and B. Schmidt[2]**

[1] Institut für Physikalische Chemie und Elektrochemie, Lehrstuhl für Theoretische Chemie, Universität Karlsruhe, Kaiserstraße 12, D-7500 Karlsruhe, Federal Republic of Germany
[2] Max-Planck-Institut für Strömungsforschung, Bunsenstraße 10, D-3400 Göttingen, Federal Republic of Germany

Optimized geometries and binding energies are calculated for ethene (ethylene) dimers, trimers, and tetramers based on a pairwise additive dimer potential. From these results intermolecular frequencies and relative abundancies (catchment areas) of the different isomers are obtained and compared with the results of accurate measurements of the photodissociation upon absorption of one photon of a CO_2 laser in the region of the v_7 monomer absorption band at 949 cm^{-1}. The clusters are size selected in a scattering experiment and show for a cluster size from $n=2$ to $n=6$ a frequency maximum shifted by 3 cm^{-1} to the blue compared with the monomer. The result is explained by the predominance of chains and chain-like structures of the clusters in the photodissociation process. The chains consist of cross-like dimer sub-units.

PACS: 36.40.01; 33.80.Gj

1. Introduction

The infrared photodissociation of ethene clusters after the excitation of the v_7 out-of-plane mode has attracted much interest in the past. The first measurements with mass spectrometer detection showed broad spectral features of about 12 cm^{-1} full width at half maximum (FWHM) [1, 2]. Later on, narrow lines were observed in high resolution studies with bolometer detection [3–6]. At the same time, the first experiments with size selected clusters were published [7–10]. They clearly demonstrated that mass spectrometry is not sufficient for mass selection of these clusters because of the large fragmentation processes during the ionisation [11]. They confirmed, however, the earlier experimental results of broad and narrow spectral features for the dimer and the overall spectra line shift of 3 cm^{-1} to the blue relative to the monomer absorption at 949 cm^{-1}. The latter result is obtained for all investigated cluster sizes both for internally cold clusters for $n=2$, 3 and 4 [8], and internally excited clusters from $n=2$ to $n=6$ [9].

In order to explain this remarkable result, we have carried out structure calculations for ethene clusters from the dimer to the tetramer based on a pair-wise additive dimer potential [12] which, in turn, was calculated using the test particle method developed by Böhm and Ahlrichs [13]. The total energy surface was then used to calculate intermolecular vibrational frequencies and, based on these results, relative abundances of certain cluster isomers as a function of temperature.

Present addresses: * BASF Aktiengesellschaft, Zentralbereich Informatik, D-6700 Ludwigshafen, Federal Republic of Germany
** Department of Chemistry, Princeton University, Princeton, NJ 08544, USA
*** Joint Institute for Laboratory Astrophysics, University of Colorado, Boulder, CO 80309, USA

In addition, the experiments were repeated in a new experimental arrangement with continuous wave CO_2-lasers [14] providing more reliable results because of the increased duty cycle by about a factor of 500. The experimental arrangement is briefly described in Sect. 2 and the resulting dissociation spectra are presented in Sect. 3. The potential calculations are outlined in Sect. 4, the normal mode analysis and population of different cluster isomers are given in Sect. 5 and 6, and the consequences for the interpretation of the spectra are discussed in Sect. 7.

2. Experiment

The $(C_2H_4)_n$ cluster beam is generated by an isentropic expansion. The preparation of size selected clusters is carried out by scattering them from a helium atomic beam. The details of the method are described in [15]. After size selection, the scattered ethene cluster beam interacts collinearly with the infrared radiation of a continuous wave CO_2-laser. The dissociation is measured by monitoring the decrease of the cluster intensity as a function of the laser frequency v and the laser fluence F. For one photon absorption processes, the fraction of dissociated molecules P_{diss} is given by

$$P_{diss} = 1 - \exp\left[-\sigma(v)\, F/h v\right] \tag{1}$$

in which σ is the dissociation cross section.

The molecular beam machine consists of two crossed beams sources at an angle of 90° which are rotatable around the scattering center [16]. The detector unit is fixed and contains a mass spectrometer where the scattered particles are first ionized by electron impact, then mass selected in a quadrupole mass filter, and finally detected by an electron multiplier. The velocity of the direct beams and the scattered particles is measured by time-of-flight (TOF) analysis using a pseudorandom technique.

The C_2H_4 cluster beam is generated from a 10% mixture in helium. The actual beam parameters are given in Table 1. From these data the Newton diagram, shown in Fig. 1, is calculated. The limiting laboratory angles for the scattering of ethene monomers to hexamers are 23.3° $(n=1)$, 11.7° $(n=2)$, 7.8° $(n=3)$,

Table 1. Beam data

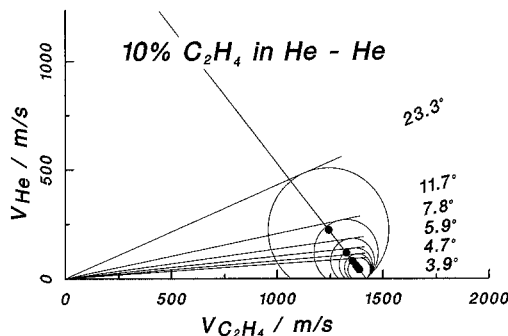|		10% C_2H_4 in He	He
Nozzle temperature	[K]	300	300
Nozzle diameter	[μm]	55	30
Pressure	[bar]	4	30
Peak velocity	[m/s]	1420	1792
Speed ratio		25.9	53.4

Fig. 1. Newton diagram for the scattering of an ethene cluster beam by a helium beam. The positions of the elastically scattered clusters from monomer to hexamer are indicated by the limiting angles in the laboratory system

5.9° $(n=4)$, 4.7° $(n=5)$, and 3.9° $(n=6)$, respectively. This angular separation of the different cluster sizes is the basis of the selection method: clusters with larger masses are excluded by kinematical constraints, while those of smaller masses are separated by the mass spectrometer. For this procedure to work, at least a small fraction of the clusters must be detected at an ion mass larger than that of the next smaller clusters. For a detailed discussion of the fragmentation behaviour by electron impact ionisation and the selection of masses we refer to [9, 11]. Typical dimer fragment masses are $m=41$ amu and 55 amu, while trimers and tetramers are detected at $m=56$ amu, and larger clusters at $m=69$ amu.

To dissociate the clusters, a homemade continuous wave CO_2-laser operating at 4 W is used. In the collinear arrangement of laser and scattered beam this power corresponds to a laser fluence of 11 mJ/cm². For a more detailed description of the laser itself as well as of the calibration of the fluence the reader is referred to [14].

3. Dissociation spectra

The photodissociation is measured by the depletion of the cluster beam upon laser radiation. The combination of scattering angles and masses which have been used for the cluster preparation are presented in Table 2 for two sets of laser gases. No. 1–6 for pure CO_2 gas and No. 7–10 for both CO_2 and N_2O gas in order to increase the number of available laser lines. The cluster composition has been determined from the measured angular distribution and time of flight analysis. For dimers and trimers pure size selection is possible. For the larger clusters mixture with one dominating cluster size are obtained. The results of the configurations No. 1–6 are shown in Fig. 2 and those of No. 7–10 in Fig. 3.

Table 2. Cluster composition of scattered beams used in the photo-dissociation experiments

No.	m/(amu)	θ/(deg)	2	3	4	5	6
1	41	9.5	100	–	–	–	–
2	56	6.0	–	100	–	–	–
3	55	5.0	4	38	58	–	–
4	55	4.4	2	22	60	16	–
5	56	4.0	–	12	50	38	–
6	69	3.5	–	–	6	29	65
7	41	9.5	100	–	–	–	–
8	56	6.5	–	100	–	–	–
9	56	5.5	–	60	40	–	–
10	55	5.0	–	–	6	29	65

Fig. 3. Dissociation spectra for $(C_2H_4)_n$ clusters with additional measurements on N_2O-laser lines marked by open circles. The exact contributions of the different cluster sizes to the spectra are listed in Table 2 and marked by the dashed line in the spectra
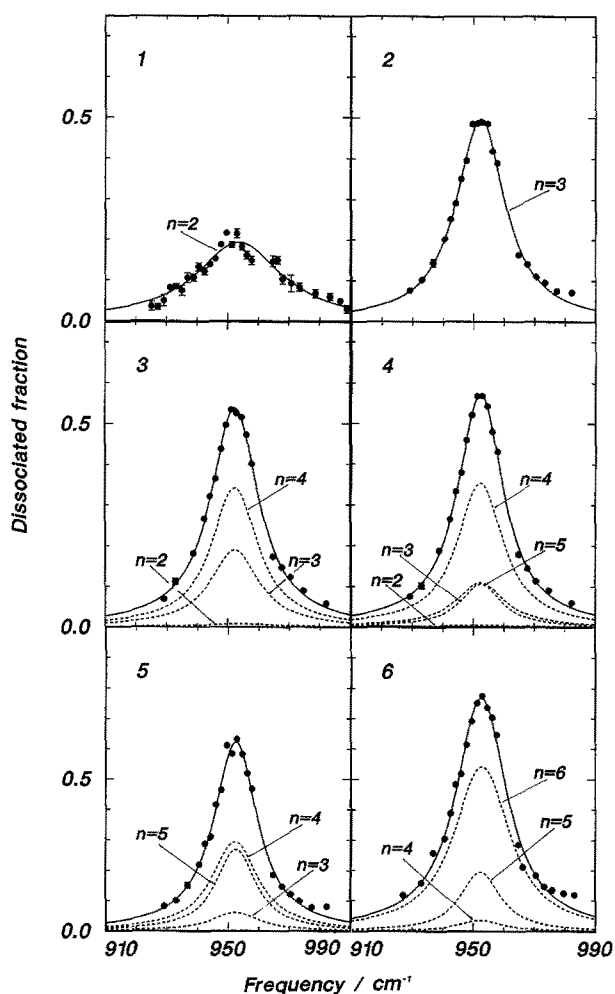

Fig. 2. Dissociation spectra for $(C_6H_4)_n$ clusters, $n = 2$–6. If more than one cluster size is present (see Table 2) the corresponding contributions to the spectrum are indicated by the dashed lines in the figure
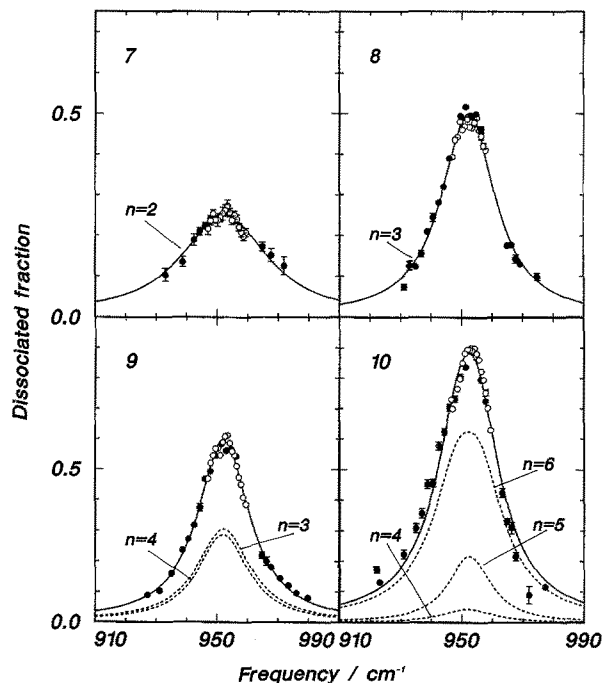
The dissociation cross section from the initial state i to the final continuum state α at the energy E is given by [17]

$$\sigma(i \to \alpha E) = \frac{4\pi^2 \omega}{c} |\langle f|\boldsymbol{\mu} \cdot \mathbf{e}|i\rangle|^2 \frac{\Gamma_f}{(E - E_f)^2 + \Gamma_f^2} \qquad (2)$$

where μ is the transition dipole moment from i to the discrete state f which then decays by the rate Γ_f to the continuum and e is the polarisation vector of the electromagnetic radiation. Therefore, the measured spectra are fitted to (1) with a Lorentzian shape for σ with three free parameters, ν_0, the maximum position, Γ, the full width at half maximum, and σ_0, the cross section at the maximum. The results of the fits which reproduce the data very well are shown as solid lines in Figs. 2 and 3. If more than one cluster size contributes to one spectrum, Eq. (1) is replaced by a sum of exponential functions and the results of the fit parameters which are already known from previous fits are used as constraints in the new fit.

The final results of both sets of data are presented in Table 3. The new, more reliable results agree on the whole with results obtained with the pulsed laser [8, 9]. The most remarkable feature is that all cluster sizes exhibit a maximum frequency of about 952.5 cm^{-1} which corresponds to a frequency shift of about 3.3 cm^{-1} to the blue and these results do

Table 3. Photodissociation data of (C_2H_4) clusters[a]

n	$\nu_0 \, [cm^{-1}]$	$\Gamma \, [cm^{-1}]$	$\sigma_0 \, [10^{-18} \, cm^2]$
2	953.2 ± 0.7	32.0 ± 2.1	0.38 ± 0.2
3	952.3 ± 0.5	17.2 ± 0.8	1.07 ± 0.10
4	952.2 ± 0.2	14.9 ± 0.3	1.62 ± 0.10
5	952.5 ± 0.1	12.1 ± 0.5	1.97 ± 0.12
6	952.5 ± 0.4	14.0 ± 0.6	3.74 ± 0.55

[a] Maximum frequency, FWHM, maximum cross section

not depend on whether internally excited [9] or cold clusters [8] are dissociated. These values are also in agreement with the experiments without size selection [1, 2], a fact which is not very surprising, since the shift does not depend on cluster size. In [1] the same value is obtained for a spectrum obtained at mass $m = 196$ amu which nominally corresponds to $n = 7$. Very probably the spectrum is caused by larger fragmented clusters $(n > 10)$ so that the frequency shifts observed for liquids $(961 \, cm^{-1})$ and solids $(969 \, cm^{-1})$ are not yet reached for these cluster sizes.

The half widths follow exactly the trend already observed for internally excited clusters with the pulsed laser system [9]. The result clearly rules out contributions of power broadening to the linewidth, since the laser power in both experiments differs by 6 orders of magnitude from 6 MW to 4 W. The linewidth is largest for the dimer, decrerases continuously and reaches the value of $12 \, cm^{-1}$ observed for cold clusters, at $n = 5$. For the detailed discussion and interpretation we refer to [9] and a forthcoming paper on the dimer [18].

The dissociation cross section at the maximum σ_0 increases with increasing cluster size. The observed decrease between tetramer and pentamer [9] is not reproduced by the present data which we think, be-
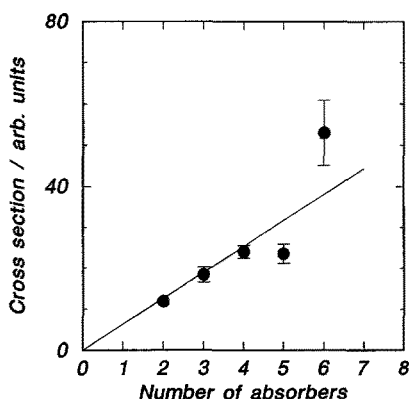
cause of the much more precise data, is the more reliable result. The cross section integrated over the Lorentzian which is proportional to $\Gamma\sigma_0$ is according to (2) a direct measure of the transition matrix element. These data are plotted in Fig. 4. Within the experimental error, a linear dependence of the transition matrix element which cluster size n is found. This result can be rationalized by assuming that the dipole moment of the cluster is given by $\mu_n = n\mu_1$ where μ_1 is the monomer value.

We conclude this experimental section by stating again the main result that the observed line shift is independent of cluster size.

4. Potential calculation

4.1. The ethene pair-potential

The pair-potential used for the theoretical investigation of ethene clusters was constructed with the help of the test particle method developed by Böhm and Ahlrichs [13, 19]: The total interaction energy for an A_2-dimer is approximated by three terms:

$$\Delta E_{AA}^{(1)} = \Delta E_{rep}^{(1)} + \Delta E_{elec}^{(1)} + \Delta E_{rest} \tag{3}$$

$\Delta E_{rep}^{(1)}$ is the first-order contribution to the electron-exchange energy. The distance and orientation-dependence is approximated by a sum of exponential site-site interactions. If i and j are sited on the two molecules, then

$$\Delta E_{rep}^{(1)} = \sum_{i,j} \exp\left(-(R_{ij} - \sigma_i - \sigma_j)/(\rho_i + \rho_j)\right), \tag{4}$$

where R_{ij} is the site-site separation. The site-specific parameters σ and ρ are obtained from ab-initio calculations at the first-order SCF level: the molecule of interest is probed with an uncharged, spherically symmetric test particle (T). Using information about the $T - T$ interaction $(\sigma_T$ and $\rho_T)$, σ_i and ρ_i are determined from a fit of (4) to the calculated energies of the molecule-T system.

The term $E_{elec}^{(1)}$ in (3) is the first-order contribution to the electrostatic energy. This is written as the sum of interactions between point charges, i.e.

$$\Delta E_{elec}^{(1)} = \sum_{i,j} q_i q_j/R_{ij}. \tag{5}$$

The site charges q are determined by probing the molecule with a unit charge, i.e. by determining the electrostatic potential which is then reproduced by a point charge model.

Fig. 4. Dissociation cross sections integrated over all frequencies as a function of the cluster size and, therefore, the number of absorbers in the cluster

The remaining term in the potential, ΔE_{rest}, gathers together the higher-order contributions to ΔE_{AA}. Only the dipole-dipole dispersion energy is taken into account, since the quadrupole-induced dipole interaction vanishes more quickly with increasing separation of the molecules:

$$\Delta E_{rest} = -\xi \sum_{i,j} C_{ij}/R_{ij}^6 \cdot F_{ij}(R_{ij}) \tag{6}$$

using

$$F_{ij}(R_{ij}) = \begin{cases} \exp\left(-(1.28 \cdot R_{vwij}/R_{ij} - 1)^2\right) \\ 1.0 \text{ else } R_{ij} < 1.28 \cdot R_{vwij} \end{cases} \tag{7}$$

as a damping function [20] for short distances, R_{vwij} being the sum of van der Waals radii for the corresponding atoms [21].

The dispersion coefficients are calculated from the atomic polarizabilities [22] α and the numbers of valence electrons N via the Slater-Kirkwood formula [23]:

$$C_{ij} \sim (3/2)\,\alpha_i\,\alpha_j \Big/ \left(\sqrt{\frac{\alpha_i}{N_i}} + \sqrt{\frac{\alpha_i}{N_j}}\right). \tag{8}$$

The remaining adjustable parameter, ξ, is obtained by fitting to the experimental second virial coefficient $B(T)$ [24].

This approach has already been applied successfully to various systems to investigate gas-phase and liquid-phase properties [19, 25–27]. Details of the application to $(C_2H_4)_2$ and the properties of liquid and solid ethene will be published elsewhere [12].

The positions of the sites are listed in Table 4; the sites labelled C and H are related to the C and H atoms in C_2H_4, Du denotes four additional dummy-centers introduced to describe the anisotropy of the repulsive and electrostatic interactions properly. Their positions – just under and above the molecular plane near to the C-sites – were chosen to allow for the contribution of π-electrons to the intermolecular potential. The numerical values of the parameters used in this work are listed in Table 5.

Table 4. Position of potential sites for ethene dimer potential[a]

Site	x_i [b]	y_i	z_i
C	1.2637	0.0	0.0
H[c]	2.3852	1.841	0.0
Du	1.3637	0.0	0.5

[a] Center of mass at origin. The positions of all other sites may be obtained using the 2-fold z-axis and the $x-y$ mirror plane
[b] In atomic units: 1 Bohr = 52.9177 pm
[c] Shifted from the H-atom position towards the C-atom by 0.05 atomic units

Table 5. Potential parameters for the ethene dimer[a]

	Site parameters			Site-site parameters	
	ρ_i	σ_i	q_i	ξC_{ij} [b]	R_{vwij}
C	–	–	+0.6	C–C	32.054	6.426
H	0.1763	0.4402	+0.178	C–H	12.314	5.482
Du	0.3636	0.3973	−0.478	H–H	4.850	4.537

[a] In atomic units: 1 Bohr = 52.9177 pm, 1 Hartree = 2625.5 kJ/mol
[b] $\xi = 1.36$

4.2. The ethene clusters

With the help of this 10-center pair-potential the equilibrium geometries and well-depths of $(C_2H_4)_2$, $(C_2H_4)_3$ and $(C_2H_4)_4$ clusters are calculated using a Monte-Carlo approach: for a sufficiently large number (~ 100) of randomly chosen starting configurations the intermolecular degrees of freedom (i.e. keeping the C_2H_4-unit rigid) are optimized by a Newton like strategy [28]. Table 6 shows the interactions energies for the most important clusters. Some selected geometries are depicted in Figs. 5, 6 and 7 for the dimer, trimer and tetramer, respectively.

The most stable dimer ($\Delta E = -6.87$ kJ/mol, D_{2d} −symmetry, Fig. 5A) consists of two crossed C_2H_4-sub units. The other structures, which show a shifted side to side arrangement (C_i, Fig. 5B) and a T-shape structure (C_{2v}, Fig. 5C) are by 1.86 and 2.73 kJ/mol less stable. This is in contrast to findings of several previous calculations, which postulate a sandwich-like structure with the molecules shifted parallel to the $C-C$ axis to be the most stable dimer. Results of this kind have been obtained by van der Avoird and coworkers [29, 30] with a minimum energy of $\Delta E = -5.01$ kJ/mol using ab initio valence bond and first and second order calculations and by Iguchi and Suzuki [31] with $\Delta E = -3.84$ kJ/mol using ab initio exchange perturbation methods. Dynamical calculations were also carried out with such a poten-

Table 6. Calculated interaction energies $|\Delta E|$ in kJ/mol for ethene clusters, their symmetries and structures[a]

Dimer				Trimer				Tetramer			
No.	ΔE	Sym	Str	No.	ΔE	Sym	Str	No.	ΔE	Sym	Str
A	6.87	D_{2d}	C	A	14.29	C_3	Ri	A	25.10	S_4	Ri
B	5.01	C_i	P	B	13.81	D_{2h}	Ch	B	23.17	C_1	Ri
C	4.14	C_{2v}	T	H	12.02	C_1	Ch	E	21.53	C_{2h}	RC
–	–	–	–	I	11.06	C_{2v}	Ch	J	20.76	D_{2d}	Ch

[a] C: cross, P: parallel, T: T-shape, Ri: ring, Ch: Chain, RC: ring with cross-like bonded units
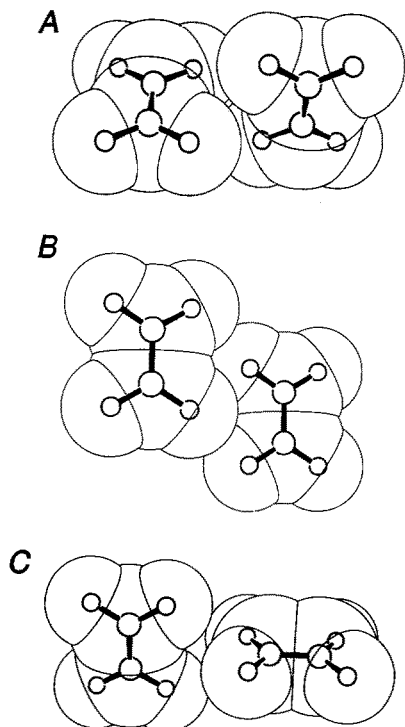
346

Fig. 5. Three different dimer configurations obtained with the new ethene pair potential. The binding energies and the symmetry groups of these isomers are listed in Table 6
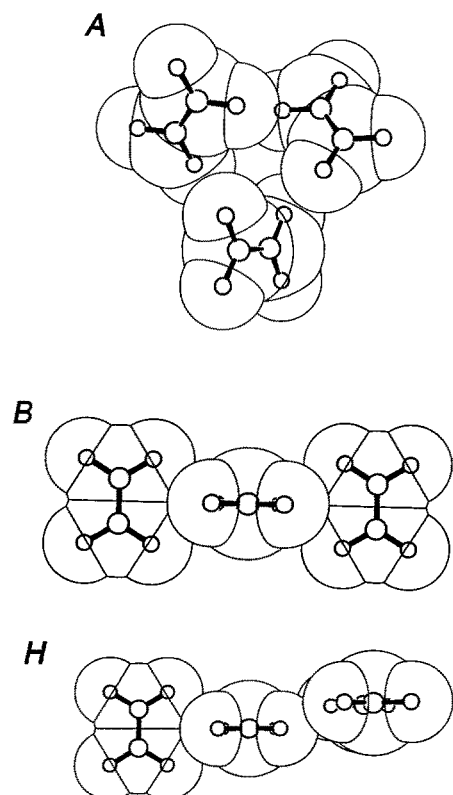

Fig. 6. Three different trimer configurations. The binding energies and the symmetry group of these isomers are listed in Table 6
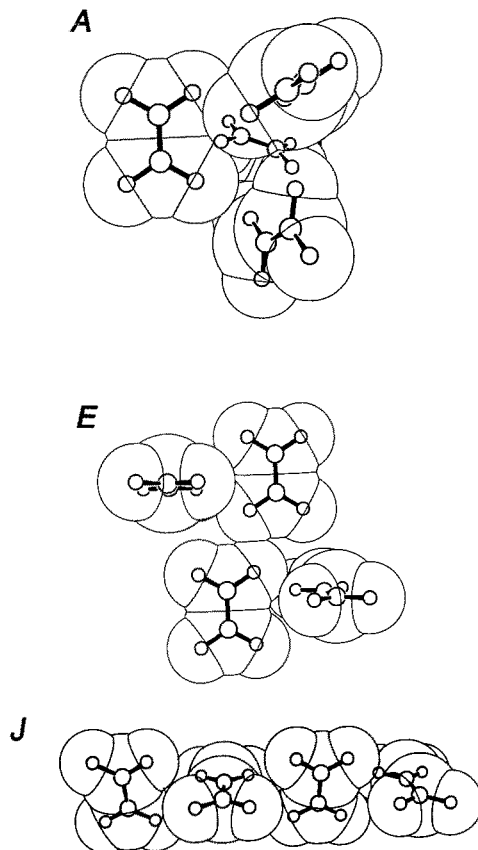

Fig. 7. Three different tetramer configurations. The binding energies and the symmetry group of these isomers are listed in Table 6

tial with an added electrostatic term [32] with $\Delta E = -5.09$ kJ/mol. It is noted that in all cases the angle between the $C-C$ axis of one molecule and the line which connects the two centers of masses varies from 45° to 68°. However, our model predicts a by 1.86 kJ/mol less favorable energy for a similar parallel shifted structure (B). To investigate this discrepancy, we have carried out CPF ab-initio calculations [33] for $(C_2H_4)_2$. The CPF-method – a size extensive modification of CI(SD) – has already provided good results in the investigation of the $(NH_3)_2$ potential surface [34, 35], if extended basis sets (including f-functions) are used. In the present work on $(C_2H_4)_2$ only a "small" basis set [36] could be used. Therefore the CPF results suffer from basis set superposition errors [37] and the slow convergence of energies with respect to the highest 1-quantum numbers of the polarization functions included in the basis set. With this method we find the same energetic order for the ethene dimers as predicted by our model. The cross-structure $(\Delta E_{CPF} = -4.50$ kJ/mol) is about 2.1 kJ/mol more stable than the shifted sandwich arrangement $(\Delta E_{CPF} = -2.4$ kJ/mol). Even if the test particle model potential seems to be too anisotropic, a hint for the

reliability of our potential model may be derived from the investigation of liquid-phase properties of ethene [12]: The reorientation-correlation times calculated by molecular-dynamics simulations of the liquid with the help of our potential are in good agreement with experimental results.

It is interesting to note that the very recent calculations of Alberts et al. [38] using the Møller-Plesset second order procedure give the deepest well $\Delta E = -5.02$ kJ/mol for the T-shape structure and $\Delta E = -4.60$ kJ/mol for the parallel configuration. These results should be compared with our configuration C and B, respectively, which give within 20% the same magnitude of the well depth but in the reversed order. Apparently the crossed structure has not been considered in the treatments mentioned above [29–31, 38].

The most stable trimer $(\Delta E = -14.29$ kJ/mol, Fig. 6A) is a ring-like arrangement with C_3-symmetry. Only 0.5 kJ/mol less stable we find a linear chain with D_{2h}-symmetry, where the C_2H_4-subunits are bound together similar to the cross dimer with a total energy of 13.81 kJ/mol (Fig. 6B). The next stable species with binding energies between 13.56 kJ/mol and 12.20 kJ/mol are ring-like structures. Configurations H (Fig. 6H) and I with energies of 12.02 kJ/mol and 11.06 kJ/mol are simply combinations of the dimer configurations A and B and A and C in a chain-like arrangement.

The lowest configuration of the tetramer is a close-packed structure with $\Delta E = -25.10$ kJ/mol (Fig. 7A) followed by a ring and a group of ring-like configurations with energies between 21.68 kJ/mol and 20.92 kJ/mol. They all have in common that at least one unit is bound similar to the cross dimer. An example with high symmetry C_{2h} is shown in Fig. 7E which exhibits two of these cross dimers. Then the first chain structure with D_{2d}-symmetry (Fig. 7J) appears $(\Delta E = -20.76$ kJ/mol) which only consists of bonds similar to the cross dimer.

5. Calculation of intermolecular frequencies

In order to calculate harmonic frequencies of the intermolecular motion as required for the population analysis put forward in Chap. 6, the standard methods of normal mode analysis [39] have to be extended to the treatment of a cluster of molecules assumed to be rigid: A particularly favorable choice is to employ three cartesian coordinates and three angles of rotation about the molecular principal axes of inertia to represent position and orientation of each monomer unit, respectively. For an aggregate of N molecules the $6N$ generalized coordinates q_i are ob-

tained by weighting displacement coordinates defined with respect to a stationary point of the potential energy surface. Cartesian displacements δx_i are weighted with the square root of the molecular mass m

$$q_i = \sqrt{m} \cdot \delta x_i, \tag{9}$$

rotational displacements $\delta \alpha_i$ are weighted with the square root of the moment of inertia, I, for rotation about the corresponding principal axis

$$q_i = \sqrt{I} \cdot \delta \alpha_i. \tag{10}$$

With this choice of coordinates the expression for the kinetic energy

$$T = \frac{1}{2} \sum_{i,j=1}^{6 \cdot N} T_{ij} \dot{q}_i \dot{q}_j \tag{11}$$

simplifies to

$$T = \frac{1}{2} \sum_{i=1}^{6 \cdot N} \dot{q}_i^2, \tag{12}$$

i.e. the metric tensor T_{ij} equals a $6N$-dimensional unit matrix. In the framework of the harmonic approximation the potential energy can be expanded in vicinity of a stationary point with binding energy ΔE

$$E = \Delta E + \frac{1}{2} \sum_{i,j=1}^{6 \cdot N} V_{ij} q_i q_j, \tag{13}$$

where the matrix elements of the second derivatives

$$V_{ij} = \frac{\partial^2 V}{\partial q_i \partial q_j}\bigg|_0 \tag{14}$$

are evaluated numerically using a three- and four-point-formula [40] for the diagonal and off-diagonal elements of the (symmetric) force constant matrix, respectively. Subsequently, the frequencies are calculated by taking the square roots of the eigenvalues of this matrix. Note that in general the V- and T-matrix have to be diagonalized simultaneously [41], which is not necessary in this case because of the extremely simple form of T given by (12). For purposes of illustration the resulting frequencies for some dimer and tetramer configurations are listed in Tables 7 and 8.

Three interesting features will be discussed more in detail: Firstly, 6 out of $6N$ frequencies must vanish, since they correspond to the translational and rotational degrees of freedom. Their values are found to be smaller than 0.1 cm^{-1}, i.e. two orders of magnitude below the lowest vibrational frequencies (or four

Table 7. Intermolecular frequencies of ethene dimers[a]

A	B	C
102.31	89.16	78.08
102.31	88.25	59.49
76.24	44.70	50.07
49.15	41.76	47.28
49.15	38.36	32.83
38.54	i23.94	i34.95

[a] Harmonic frequencies [in cm^{-1}] for dimers of rigid molecules. Note the two pairs of degenerate frequencies for dimer A and the imaginary frequencies for dimers B and C

Table 8. Intermolecular frequencies of ethene tetramers[a]

A	E	J
109.12	113.83	143.35
100.01	111.62	143.35
100.01	99.88	101.20
99.68	91.97	101.20
94.35	85.77	100.56
88.02	84.14	76.62
71.84	72.87	68.06
60.73	60.89	68.06
60.73	53.43	50.52
59.11	47.10	49.73
46.58	43.64	49.73
44.31	42.07	41.46
39.28	35.44	37.89
39.28	31.62	22.34
32.89	27.93	22.34
29.79	20.57	19.84
29.79	17.00	9.98
21.95	12.25	9.98

[a] Harmonic frequencies [in cm^{-1}] for tetramers of rigid molecules. Note the occurrence of four and six pairs of degenerate frequencies for tetramers A and J, respectively

orders of magnitude for the eigenvalues of V) thus confirming the acuracy of our calculations. Secondly, one imaginary frequency occurs for the dimer configuration B and C. This indicates that these stationary points do not represent unconditional minima but rather can be thought of as saddle points or ridges of the potential energy surface. It is interesting to compare the results for structures B and C with similar calculations of [38]. In the case of the parallel structure B the results are quite similar, 5 real frequencies in the range of 121 to 42 cm^{-1} and one imaginary at i 16 cm^{-1}. For the T-shaped structure a real minimum was found in contrast to the present study. Thirdly there are degenerate frequencies for some symmetric cluster configurations. To calculate these degeneracies, the group theoretical methods for the treatment of intermolecular vibrations [42] have to be modified slightly for the case of intermolecular vi-

brations: For each symmetry operation R contained in the appropriate symmetry point group, a $6N$-dimensional matrix representing the transformation of the basis set introduced above has to be set up: The traces of these matrices yield $n_R \chi_R$, where n_R is the number of molecules that are left unchanged under symmetry operation R and χ_R can be shown to be 6 for E, $2+4 \cos 2\pi k/n$ for C_n^k, $-2+4 \cos 2\pi k/n$ for S_n^k, -6 for i and zero for σ. After decomposing this (reducible) representation into irreducible representations ("irreps") and deleting those corresponding to rotation and translation, one finally obtains the number of times a certain irrep occurs in the representation of the genuine normal modes. Since all symmetric configurations under consideration can be assigned to C-, D- or S-groups, no higher than twofold degeneracies can occur (see Tables 7 and 8). The numerical results are in remarkably good agreements with these considerations, the degenerate frequencies are identical to five to seven digits.

Furthermore our calculated frequencies can be compared with previous experiments and calculations. Snels et al. [3] measured a combination band of the v_7 mode and a van der Waals mode of 36 cm^{-1}. This value compares well with our lowest frequency of 38.5 cm^{-1} for dimer A which corresponds to the torsional motion about the intermolecular axis. However, it is difficult to compare our results with other calculations in which either in a vibrational close-coupled IOS method only one azimuthal bending mode is considered [43] or the energy levels of uncoupled local modes are calculated [44]. Both calculations refer to a parallel shifted minimum configuration [32] which is completely different from our structure A. Therefore it is interesting to repeat these calculations with the potential model of this work.

6. Population of different isomers

For finite tempertures clusters are not only confined to the energetically lowest configuration but rather tend to explore higher regions of their configurational space. That process of thermal averaging can be modeled by means of computer simulation: Two techniques originally developed for the studies of fluids, the Monte-Carlo (MC) and the molecular-dynamics (MD) methods, have become useful tools for theoretical investigations of the thermodynamic properties of clusters. In order to avoid the computational efforts inherent to those methods, we decided to apply a considerably simpler approach proposed by Hoare [45]: The potential hypersurface can be thought of to be divided into "catchment regions" of its local minima. Such a region is the subset of points from

where steepest-descent trajectories lead to a certain minimum. The intermolecular frequencies give a rough measure of such a region: high frequencies indicate a narrow potential well, while low frequencies indicate a wide and flat catchment region. To determine the relative population of these regions, the canonical partition function Z for the corresponding minima has to be set up supposing the cluster to behave like a rigid rotor and the intermolecular vibrations to be harmonic. Note that the latter assumption is equivalent to the Debye model common in solid state physics. From this the expression for the Helmholtz free energy can be calculated easily

$$F = U - TS = -k_B \ln Z. \tag{15}$$

One finally obtains the relative probabilities for finding the system in the vicinity of either minimum 1 or 2 given by

$$\frac{P^{(2)}}{P^{(1)}} = \exp\left(-\frac{\Delta E^{(2)} - \Delta E^{(1)}}{k_B T}\right) \cdot \exp\left(-\frac{\varepsilon^{(2)} - \varepsilon^{(1)}}{k_B T}\right)$$
$$\cdot \sqrt{\frac{I_A^{(2)} \cdot I_B^{(2)} \cdot I_C^{(2)}}{I_A^{(1)} \cdot I_B^{(1)} \cdot I_C^{(1)}}} \cdot \prod_{i=1}^{6N-6} \left(\frac{1 - \exp(-h\nu_i^{(1)}/kT)}{1 - \exp(-h\nu_i^{(2)}/kT)}\right), \tag{16}$$

where ΔE are the well depths (counted negative), ε are the zero point energies, I_A, I_B, I_C are the principal moments of inertia, and the ν_i are intermolecular frequencies of the two minima under consideration denoted by the superscripts 1 and 2. The index i for the multiple product ranges from 1 to $6N-6$ accounting for the number of vibrational degrees of freedom of a system of N rigid molecules.

Equation (16) illustrates the interplay of two competing effects: The first two terms reflects the propensity to occupy the energetically lowest possible configuration describing the behaviour for $T \to 0$, while the forth term gives the behaviour for non-zero temperatures: For entropic reasons there is a tendency to prefer shallow minima with low frequencies, i.e. those with a large catchment region over steep deeper ones. A natural example is the relative concentration of chain-like and ring-like isomers of small molecular clusters: While rings are usually stronger bonded, chains are generally more floppy with respect to some degrees of freedom and therefore are favored for sufficiently high temperatures over the first ones as has been demonstrated by Martin et al. for the example of $(LiI)_2(CH_3OH)_2$ [46]. The third term shows the preference of spatially more extended mass distributions because of their higher entropy, too. However, it does not differ substantially from unity.

We applied this kind of statistics for assessing relative probabilities to some different isomers of small
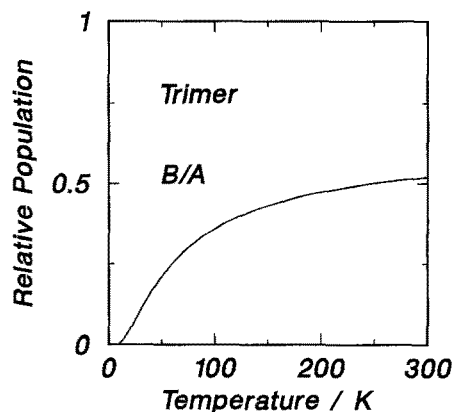
Fig. 8. Relative population of the ring-like trimer (A) and the chain-like trimer (B) as a function of temperature
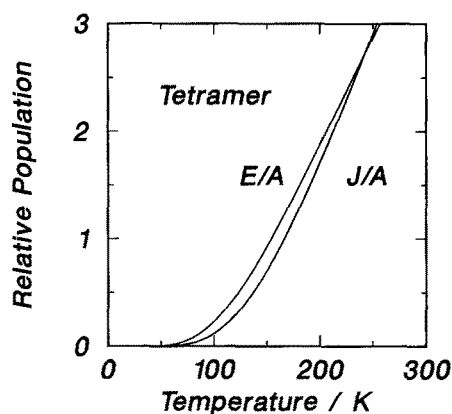
Fig. 9. Relative population of the tetramer configurations A and E and the configurations A and J as a function of temperature

ethene clusters using the new potential surface described in Chap. 4. Because of the modest number of local minima ranging between 3 for the dimer and about 15–20 for the tetramer this method is still practicable, while for more complicated cases a full simulation may prove necessary. Figure 8 gives an impression of the temperature dependency of occupation numbers for the two most stable trimer configurations, a ring (A) and a chain (B), while Fig. 9 shows the abundancies of three tetramer configurations, the ring (A), the almost flat structure (E) and the chain (J).

7. Discussion

Before we start the discussion of how to relate the results of the structure calculations to the experimental data, let us recall the main result. All photodissociation spectra in the region of the ν_7 out-of-plane vibration (B_{1u}) at 949 cm^{-1} are shifted by about 3 cm^{-1} to the blue, independent of the cluster size

350

from $n=2$ to $n=6$. One possible explanation is the existence of similar structures and energetics for the different cluster sizes. Therefore, there are essentially two aspects of the calculation which have to be considered. One is concerned with the dissociation process itself and is based on the interaction potential and the energetics calculated in Sect. 4. The other is the probability to find different isomers calculated in Sect. 6.

The dimer is a clear cut case. In our calculation the cross structure A is the only minimum with completely real frequency spectrum. The other configurations are stationary points corresponding to saddle points or transition states with imaginary frequencies corresponding to intermolecular motions which twist the C_2H_4 units into the cross structure. Therefore we attribute the experimental result entirely to the dissociation of the structure A.

The easiest explanation for the same frequency shift of the larger clusters is that, also in these cases, the same type of bond is broken with the same bonding energy. Such structures are, indeed, found in the calculations, the chains of configuration B for the trimer and J for the tetramer. To dissociate these clusters, only one bond has to be broken and the bonding energy is in all cases 6.90 kJ/mol as is found for the dimer.

For the trimer the chain configuration B is only the second lowest in energy about 0.5 kJ/mol apart from the ring configuration A. The population analysis shows that, whatever the cluster temperature may be, the relative probabilities of structure B is only 0.6 of the ring configuration A. In the latter case, however, two bonds have to be broken to dissociate this cluster, a process which requires at least 7.4 kJ/mol if a molecule and dimer A are formed. For any other product dimer this energy is even larger. This is probably the reason why structure B is preferred in the dissociation.

In the case of the tetramer the chain structure J has a bonding energy which is lower by 4.34 kJ/mol compared with the most stable minimum, the configuration A. Although the energetics are again in favor for the dissociation of the chains – the necessary energy to remove one unit is 6.92 kJ/mol for the chain compared with at least 10.8 kJ/mol for the ring – the difference of the minimum energies seems to be too large to compensate for this effect. In this case, however, the population analysis clearly demonstrates that at values larger than 180 K the relative probability to find configuration J compared with A becomes larger than one.

Now we have to address the complicated question of the actual cluster temperature. There are two different effects which determine this temperature during the process of cluster formation, the collisional cooling and the evaporative cooling [47]. For dimers of atoms or diatoms spectroscopic methods were used indicating different temperatures for rotational and vibrational degrees of freedom as in the case of molecules. The only other source of information for larger clusters are electron diffraction measurements averaged over a number of amorphous structures obtained by Molecular Dynamics simulations [48]. The results of these experiments for different van der Waals clusters, which have similar structures as the solid state, show a correlation of the temperature T_{Cl} with the well depth ΔE of the dimer with $T_{Cl} \approx 0.33|\Delta E|/k_B$. If we take the result of the present calculation for ΔE, we end up with $T_{Cl}=274$ K. Even if we take into account that the calculated ΔE might be too large and we have in addition to lower the value since we are dealing here with relatively small tetramers, $T_{Cl}=200$ K is apparently a reasonable value for the cluster temperature so that indeed the chain structure J is found preferentially in the beam. In addition, we note that all the sructures from C to I contain C_2H_4-units bound in a similar way to the cluster as the cross dimer and that also these structures, as is demonstrated for the E/A ratio in Fig. 9 appear with larger probabilities than structure A in the population analysis for $T_{Cl}>180$ K. All these findings clearly demonstrate that the experimental results of the line shift are best explained by the fact that chains or chain-like structures which contain at least one of the cross type bonds of the ethene dimer are essentially responsible for the dissociation. Of course, direct calculations of the line shift for the different clusters and their isomers, which are underway in our group, will finally give a complete answer for this problem.

References

1. Casassa, M.P., Bomse, D.S., Janda, K.C.: J. Chem. Phys. 74, 5044 (1981)
2. Hoffbauer, M.A., Liu, K., Giese, C.F., Genty, W.R.: J. Chem. Phys. 78, 5567 (1983)
3. Snels, M., Fantoni, R., Zen, M., Stolte, S., Reuss, J.: J. Chem. Phys. 124, 1 (1986)
4. Baldwin, K.G.H., Watts, R.O.: Chem. Phys. Lett. 129, 237 (1986)
5. Baldwin, K.G.H., Watts, R.O.: J. Chem. Phys. 87, 873 (1987)

6. Heijmen, B., Liedenbaum, C., Stolte, S., Reuss, J.: Z. Phys. D – Atoms, Nuclei and Clusters **6**, 199 (1987)
7. Huisken, F., Meyer, H., Lauenstein, Ch., Sroka, R., Buck, U.: J. Chem. Phys. **84**, 1042 (1986)
8. Huisken, F., Pertsch, T.: J. Chem. Phys. **86**, 106 (1987)
9. Buck, U., Huisken, F., Lauenstein, Ch., Meyer, H., Sroka, R.: J. Chem. Phys. **87**, 6276 (1987)
10. Buck, U., Lauenstein, Ch., Rudolph, A., Heijmen, B., Stolte, S., Reuss, J.: Chem. Phys. Lett. **144**, 396 (1988)
11. Buck, U., Lauenstein, Ch., Meyer, H., Sroka, R.: J. Phys. Chem. **92**, 1916 (1988)
12. Brode, S., Ahlrichs, R., Kathan, B., Karch, B.: (in preparation); Brode, S.: Dissertation, Universität Karlsruhe FRG (1988)
13. Böhm, H.J., Ahlrichs, R.: J. Chem. Phys. **77**, 2088 (1982)
14. Buck, U., Gu, X.J., Lauenstein, Ch., Rudolph, A.: J. Chem. Phys. (1990)
15. Buck, U.: J. Phys. Chem. **92**, 447 (1988)
16. Buck, U., Huisken, F., Schleusener, J., Schaefer, J.: J. Chem. Phys. **72**, 512 (1980)
17. Beswick, J.A.: In: Structure and dynamics of weakly bound molecular complexes. Weber, A. (ed.), p. 563. Dordrecht: Reidel 1987
18. Buck, U., Lauenstein, Ch., Rudolph, A.: Z. Phys. D. (in preparation)
19. Böhm, H.J., Ahrichs, R., Scharf, P., Schiffer, H.: J. Chem. Phys. **81**, 1389 (1984)
20. Ahlrichs, R., Penco, R., Scoles, G.: Chem. Phys. **19**, 119 (1977)
21. Bondi, A.: J. Phys. Chem. **68**, 441 (1964)
22. Ketelaar, J.A.A.: Chemical constitution. New York: Elsevier 1957
23. Slater, J.C., Kirkwood, J.G.: Phys. Rev. **37**, 682 (1931)
24. Dymond, J.H., Smith, E.B.: The virial coefficients of pure gases and mixtures. Oxford 1981
25. Böhm, H.J., Meissner, C., Ahlrichs, R.: Mol. Phys. **53**, 651 (1984)
26. Sagarik, K.P., Ahlrichs, R.: J. Chem. Phys. **86**, 5117 (1987)
27. Brode, S., McDonald, I.R.: Mol. Phys. **65**, 1007 (1988)
28. The quasi-Newton algorithm which is implemented in the NAG-library subroutine E04JAF was used
29. Wasiutynski, T., van der Avoird, A., Berns, R.M.: J. Chem. Phys. **69**, 5288 (1978)
30. Avoird, A. van der, Wormer, P.E.S., Mulder, F., Berns, R.M.: Topics Curr. Chem. **93**, 1 (1980)
31. Suzuki, K., Iguchi, K.: J. Chem. Phys. **77**, 4594 (1982)
32. Peet, A.C., Clary, D.C., Hutson, J.M.: Faraday Discuss. Chem. Soc. **82**, 327 (1986)
33. Ahlrichs, R., Scharf, P., Ehrhardt, C.: J. Chem. Phys. **82**, 890 (1985)
34. Sagarik, K., Ahlrichs, R., Brode, S.: Mol. Phys. **57**, 12467 (1986)
35. Nelson, D.D. Jr., Klemperer, W., Fraser, G.T., Lovas, F.J., Suenram, R.D.: J. Chem. Phys. **87**, 6364 (1987)
36. C: $10\,s\,6p$ [511111], [411], $1d\ \eta = 0.7$, H: $6s$ [411], $1p\ \eta = 0.4$
37. Boys, S.F., Bernardi, F.: Mol. Phys. **19**, 553 (1970)
38. Alberts, I.L., Rowlands, T.W., Handy, N.C.: J. Chem. Phys. **88**, 3811 (1988)
39. Wilson, E.B., Decius, J.C., Cross, P.C.: Molecular vibrations. New York: McGraw Hill 1955
40. Schiller, W.S., Spackman, M.A.: Chem. Phys. Lett. **151**, 547 (1988)
41. Goldstein, H.: Classical mechanics, Chap. 10. Cambridge: Addison-Wesley 1961
42. Cotton, F.A.: Chemical applications of group theory. New York: Wiley Interscience 1963
43. Peet, A.: Chem. Phys. Lett. **132**, 32 (1986); Ph. D. Thesis, University of Cambridge (1987)
44. Hair, S.R., Beswick, J.A., Janda, K.C.: J. Chem. Phys. **89**, 3970 (1988)
45. Hoare, M.R.: In: Advances in chemical physics. Prigogine, L., Rice, S.A. (eds.), Vol. XL. New York: J. Wiley & Sons 1979
46. Martin, T.P., Bergmann, T., Wassermann, B.: In: Large finite systems. Proceedings of the 20th Jerusalem Symposium on Quantum Chemistry and Biochemistry. Jortner, J., Pullmann, B. (eds.). Dordrecht: Reidel 1987
47. Kappes, M., Leutwyler, S.: In: Atomic and molecular beam methods. Scoles, G. (ed.), Chap. 15, p. 380. New York: Oxford University Press 1988
48. Farges, J., Ferandy, M.F. de, Raoult, B., Torchet, G.: Surf. Science **106**, 95 (1981)